

PAPER • OPEN ACCESS

Ion milling-induced crystalline phases precipitation in multicomponent Zr-based amorphous alloys

To cite this article: Yuting Feng *et al* 2021 *J. Phys.: Conf. Ser.* **2044** 012058

View the [article online](#) for updates and enhancements.

You may also like

- [Photocatalytic Synthesis of Silver-Oxide Clathrate \$\text{Ag}_2\text{O}\cdot\text{NO}_2\$](#)

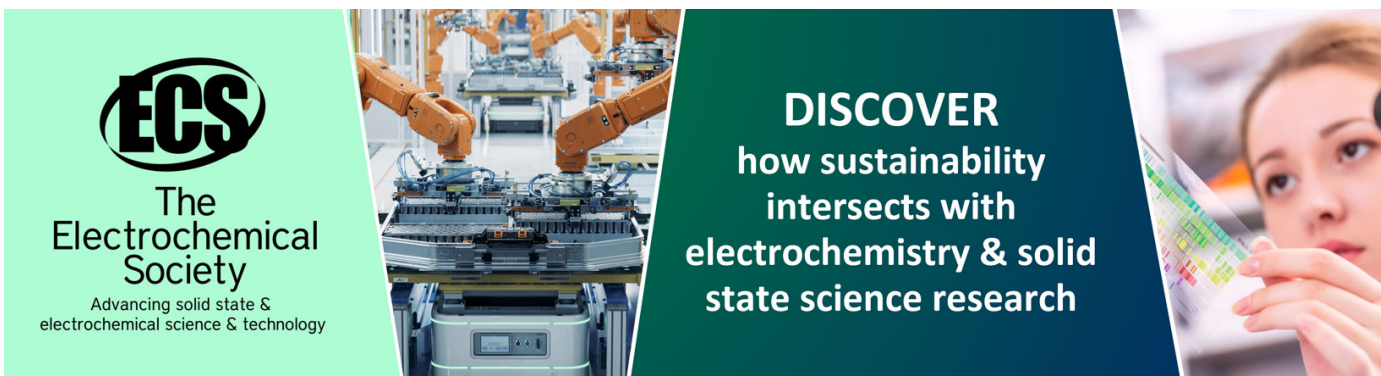
R. Tanaka, S. Takata, M. Katayama et al.

- [Charge-Transfer Luminescence and Energy Transfer in \$\text{Eu}^{2+}\$ -Doped Barium Zirconosilicates](#)

De-Yin Wang, Ling-Li Wang, Te-Ju Lee et al.

- [Structural, thermal and optical characteristics of \$\text{Fe}_{1-x}\text{Zr}_x\$ alloy by using mechanical milling approach: influence of \$\text{Zr}^{4+}\$ ion](#)

V M Illayaraja Muthaiyaa, T Parameshwaranpillai, A Krishnamoorthy et al.



ECS
The Electrochemical Society
Advancing solid state & electrochemical science & technology

DISCOVER
how sustainability intersects with electrochemistry & solid state science research

Ion milling-induced crystalline phases precipitation in multicomponent Zr-based amorphous alloys

Yuting Feng¹, Jinhua Ding², Jiawei Li³, Jing Ding^{*4}

¹School of Mechanical Engineering, Tianjin Sino-German University of Applied Sciences, Tianjin, 300072, China

²School of Mechanical Engineering, Shandong University of Technology, Zibo, Shandong, 255049, China

³Aerospace Institute of Advanced Materials & Processing Technology, Beijing, 100071, China

⁴School of Materials Science and Engineering, Tianjin University, Tianjin, 300072, China

*Corresponding author's e-mail: dingjing2017@tju.edu.cn

Abstract: Five groups of transmission electron microscopy (TEM) specimens of $Zr_{65}Al_{7.5}Co_{22.5}Ag_5$ and $Zr_{65}Al_7Co_7Ag_7Fe_7Ni_7$ amorphous ribbons are prepared by ion milling. It focuses on effect of ion milling conditions on the structure changes of amorphous ribbons. The results show that Zr-based amorphous ribbons can be crystallized into nanoscale fcc-Ag or fcc- Zr_2M (M=Al, Co, Ag, Fe, Ni) under specific ion milling conditions. The crystallization reaction sequence of isothermal annealing $Zr_{65}Al_{7.5}Co_{22.5}Ag_5$ and $Zr_{65}Al_7Co_7Ag_7Fe_7Ni_7$ amorphous alloys is different. Besides of ion beams irradiation-induced stresses and surface effects, sputtering, argon ions implantation and irradiation damages, ion irritation effect and mixing heats among constituent elements are significant, resulting in fcc-Ag or fcc- Zr_2M precipitates from amorphous phase. The peak temperature locally reached of TEM foil during ion milling is estimated more than 750K.

1. Introduction

Transmission electron microscopy (TEM) is a powerful tool to study the microstructure, crystallization behavior and shear bands patterns for amorphous materials. TEM test specimens are usually prepared by ion milling and electropolishing. Ion milling is a process in which ions collide with neutral particles. There are risks such as material transmission from one point to another under the ion beam, sputtering, argon ion implantation, chemical diffusion, thermal damage, and radiation damage^[1].

Ion milling was found to cause the transformation of amorphous phase to nanocrystalline phase. It has been reported that the $Zr_{52.5}Cu_{17.9}Ni_{14.6}Al_{10}Ti_5$ metallic glass transformed to various ordered structures during ion milling, and the peak temperature is estimated to locally reach as high as 780K^[2]. The general problem of sample heating during ion milling has been addressed by several authors^[3-7]. However, almost all earlier studies have focused on ion milling effect leading to crystal to amorphization transformation, though amorphous alloys used for the study haven't been selected. Therefore, it is of great significance to study the microstructure stability and phase transition of the



amorphous phase during ion milling. The alloys are chosen from Zr-Al-Co-Ag and Zr-Al-Co-Ag-(Fe,Ni) systems. Ternary Zr-Al-Co system is one of the most important and well-recognized systems that developed by Inoue group^[8]. Alloying with appropriate amounts of Ag changes the chemical and topological short-range orderings of Zr-Al-Co alloys, resulting in an increase of local packing efficiency and the difficulty of atomic rearrangement. As a result, Zr-Al-Co-Ag glassy alloys exhibit high thermal stability^[9]. Pseudo-high entropy Zr-Al-(Fe, Co, Ni, Cu, Ag, Pd) glassy alloy have also significantly increased thermal stability. In this paper, we studied the microstructural stability, crystallization behavior and microstructural changes in $Zr_{65}Al_{7.5}Co_{22.5}Ag_5$ and $Zr_{65}Al_7Co_7Ag_7Fe_7Ni_7$ amorphous alloys during ion milling in comparison with annealing-induced crystallized structure and to clarify the difference in the ion milling-induced structure and the anneal-induced structure, and to investigate the reason for the distinct difference. There are no data on the comparison of the structure on the multicomponent amorphous alloys subjected to such different two treatments. Furthermore, most failures of materials occur on surfaces, including fatigue fracture, fretting fatigue, wear and corrosion etc., which are very sensitive to the structure and properties of the material surface^[10]. The unique structure produced by ion milling is expected to be a new type of surface modification method to improve the global behavior of structural and functional materials.

2. Experimental Methods

The two alloys have nominal compositions (in at.%) of $Zr_{65}Al_{7.5}Co_{22.5}Ag_5$ and $Zr_{65}Al_7Co_7Ag_7Fe_7Ni_7$. Ingots were prepared by arc-melting mixtures consisting of elemental metals with purities above 99.8 mass% in an argon atmosphere. Alloy ribbons with a thickness of 0.03-0.034 mm and a width of 1.2 mm were prepared by the melt spinning method. Amorphous structure was identified by X-ray diffraction with Cu-K α radiation and transmission electron microscopy (TEM). Thermal stability associated with glass transition and crystallization temperature was examined by differential scanning calorimetry (DSC) at a heating rate of 0.67 K/s. Crystallization structure was examined by X-ray diffraction, TEM and high resolution TEM.

Five groups (A, B, C, D and E) of TEM observation foils were prepared from as-spun ribbons. TEM thin foil preparation methods and conditions for five groups were listed in Table1. The specimens in Group A were ion milled for 2.5h at 4KeV, 8°, followed by 15min milling at 2KeV, 4°. Group B specimens were ion milled at 4KeV, 8° for 3.5h, also followed by 15min milling at 2KeV, 4°. Group C specimens were ion milled at 2KeV, 4° for 8.5h. Group D specimens were dimpled to just perforate (Gatan 656 Dimple Grinder) and ion milled at 1.5 keV, 4°for about 2h; Group E specimens were dimpled to just perforate and ion milled at 1.5 keV, 4°for about 3h.

Table1 TEM specimen preparation methods and conditions for five groups

Group	Materials	Procedure	Ion beam energy +Milling time + gun angle
A	$Zr_{65}Al_{7.5}Co_{22.5}Ag_5$	Ion milling	4Kev for 2.5h, 8°; 2Kev for 15min, 4°
B	$Zr_{65}Al_7Co_7Ag_7Fe_7Ni_7$	Ion milling	4Kev for 3.5h, 8°; 2Kev for 15min, 4°
C	$Zr_{65}Al_7Co_7Ag_7Fe_7Ni_7$	Ion milling	2Kev for 8.5h, 4°
D	$Zr_{65}Al_{7.5}Co_{22.5}Ag_5$	Dimple+ Ion milling	1.5Kev for 2h, 4°
E	$Zr_{65}Al_7Co_7Ag_7Fe_7Ni_7$	Dimple+ Ion milling	1.5Kev for 3h, 4°

Ion milling processes were performed using the Gatan Precision Ion Polishing System (Gatan PIPS II 695) in the dual modulation mode and by a liquid nitrogen cold stage with PIPS holders-DuoPosts. The specimens were pasted using an electrically and thermally conducting carbon-containing glue. The stability of the gun voltage and current was monitored during ion milling.

3. Results

Fig. 1a shows XRD patterns of as-spun $Zr_{65}Al_{7.5}Co_{22.5}Ag_5$ (alloy 1[#]) and $Zr_{65}Al_7Co_7Ag_7Fe_7Ni_7$ (alloy 2[#]) alloy ribbons. Each of them has broad diffuse peaks characteristic of an amorphous structure. Fig. 1b shows DSC curves of as-spun $Zr_{65}Al_{7.5}Co_{22.5}Ag_5$ and $Zr_{65}Al_7Co_7Ag_7Fe_7Ni_7$ alloy ribbons at a heating rate of 0.67K/s. The DSC curves show no glass transition for the two alloys, and both of them have a two-stage crystallization process. The alloy 1[#] shows the crystallization peak temperature at 727K, which is lower than that (749K) for the alloy 2[#].

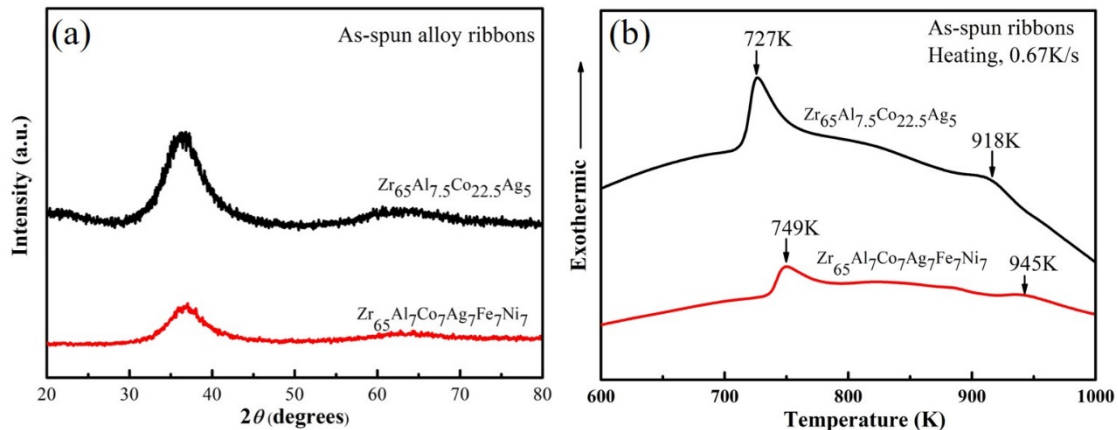


Fig. 1. (a) XRD patterns of as-spun $Zr_{65}Al_{7.5}Co_{22.5}Ag_5$ and $Zr_{65}Al_7Co_7Ag_7Fe_7Ni_7$ alloy ribbons and (b) DSC curves of crystallization process.

The Kissinger equation is usually used to estimate the apparent activation energy for the first-stage crystallization. The crystallization of amorphous phase requires long-range rearrangement of unlike atoms, during which atoms have to overcome the binding energy with neighbors to take their lattice positions [11-13]. The lower activation energy for crystallization means that crystal precipitates more easily from amorphous phase when absorbing external energies. In Fig. 2, the activation energy E is 370kJ/mol for $Zr_{65}Al_7Co_7Ag_7Fe_7Ni_7$ alloy, which is lower than that (390kJ/mol) for $Zr_{65}Al_{7.5}Co_{22.5}Ag_5$ alloy. $Zr_{65}Al_7Co_7Ag_7Fe_7Ni_7$ alloy, suggesting that the structure change during the process of ion milling is easier for the alloy 1[#].

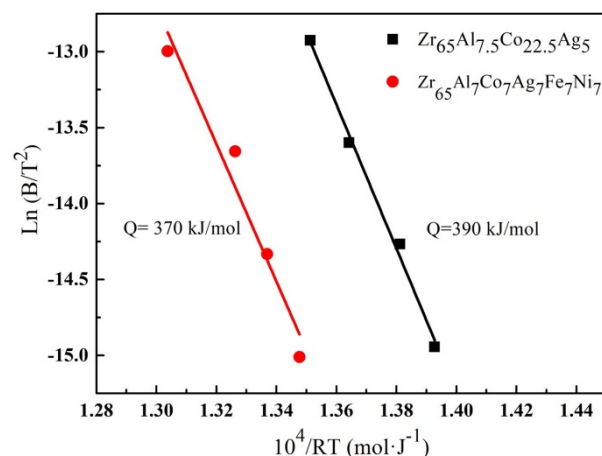


Fig. 2 Kissinger's plot of T_p for $Zr_{65}Al_{7.5}Co_{22.5}Ag_5$ and $Zr_{65}Al_7Co_7Ag_7Fe_7Ni_7$ alloy

In order to compare the crystallization phase induced by ion milling with that induced by annealing, alloys were annealed at temperatures above the first exothermic peak (750 K) and second

exothermic peak (970 K) on the DSC curves (Fig. 1(b)). As displayed in Fig. 3, there are no changes in X-ray diffraction patterns after annealing for 3.6 ks at 750 K for both alloys. Similar results have been obtained for ZrAlNiCuAg^[14], ZrAl(Fe,Co,Ni,Cu,Ag,Pd)^[15] and ZrAlNiAg^[16] alloy and the structural feature of their multicomponent and pseudo-high entropy glassy alloys have been named as clustered glassy phase^[17]. The clustered glassy phase has been defined in the satisfaction of the following factors, i.e., no changes in XRD pattern, high resolution TEM image and nanobeam electron diffraction pattern after annealing for the long time up to at least 14.4 ks at the temperature above the first exothermic peak on DSC curves^[9]. It can deduce that these two alloys are much stable when annealing temperature is below 750K. Annealing of Zr₆₅Al₇Co₇Ag₇Fe₇Ni₇ alloy at 970K for 1.8ks, [fcc-Zr₂M, Zr₂Al₃+ZrAg +Al₁₃Co₄+Al₃Zr+Zr₆CoAl₂] forms instantly from the residual amorphous phase. For Zr₆₅Al_{7.5}Co_{22.5}Ag₅ alloy, the phase mixture generated above the second peak is [Zr₂Al₃+AlAg₃+ZrAg+Al₁₃Co₄+Al₃Zr].

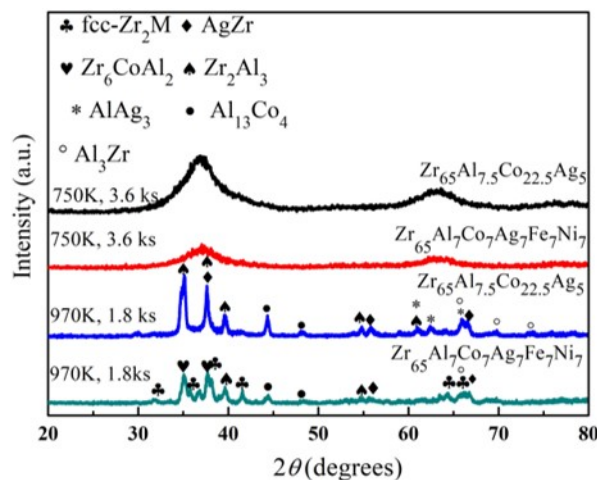


Fig. 3 X-ray diffraction patterns of Zr₆₅Al_{7.5}Co_{22.5}Ag₅ and Zr₆₅Al₇Co₇Ag₇Fe₇Ni₇ alloy ribbons annealed at a temperature above the first exothermic peak for 3.6ks and a temperature above the second exothermic peak for 1.8ks.

TEM specimens of Group A, B and C are prepared by ion milling. After ion milling, the structures of Group A, B, and C samples were changed from amorphous single phase to a coexistent phase with spherical morphology (Fig. 4a). As shown in Fig. 4a and Fig. 4b, nanoparticles appear in the specimens of Group A. These nanoparticles are uniformly dispersed and are identified as fcc-Ag phase with fine size in the range of 3-5nm (Fig. 4c). For Group B specimen, clear crystal lattice fringes can be seen in Fig. 4 e. The fast Fourier-transform (FFT) pattern (Fig. 4f) indicates that the precipitates are fcc-Zr₂M (M=Al,Co,Ag,Fe,Ni), while the main phase is still amorphous phase. Ion milling time reaches 8.5 hours for Group C specimen. The analysis results of selected area electron diffraction (SAED) patterns (Fig. 4 i) indicate that the precipitates are still cubic Zr₂M. It is interesting to note that all the crystallites phases are fcc-Zr₂M for Zr₆₅Al₇Co₇Ag₇Fe₇Ni₇ amorphous alloy, which are same with one of the phases formed upon annealing treatment when the annealing temperature is 970K.

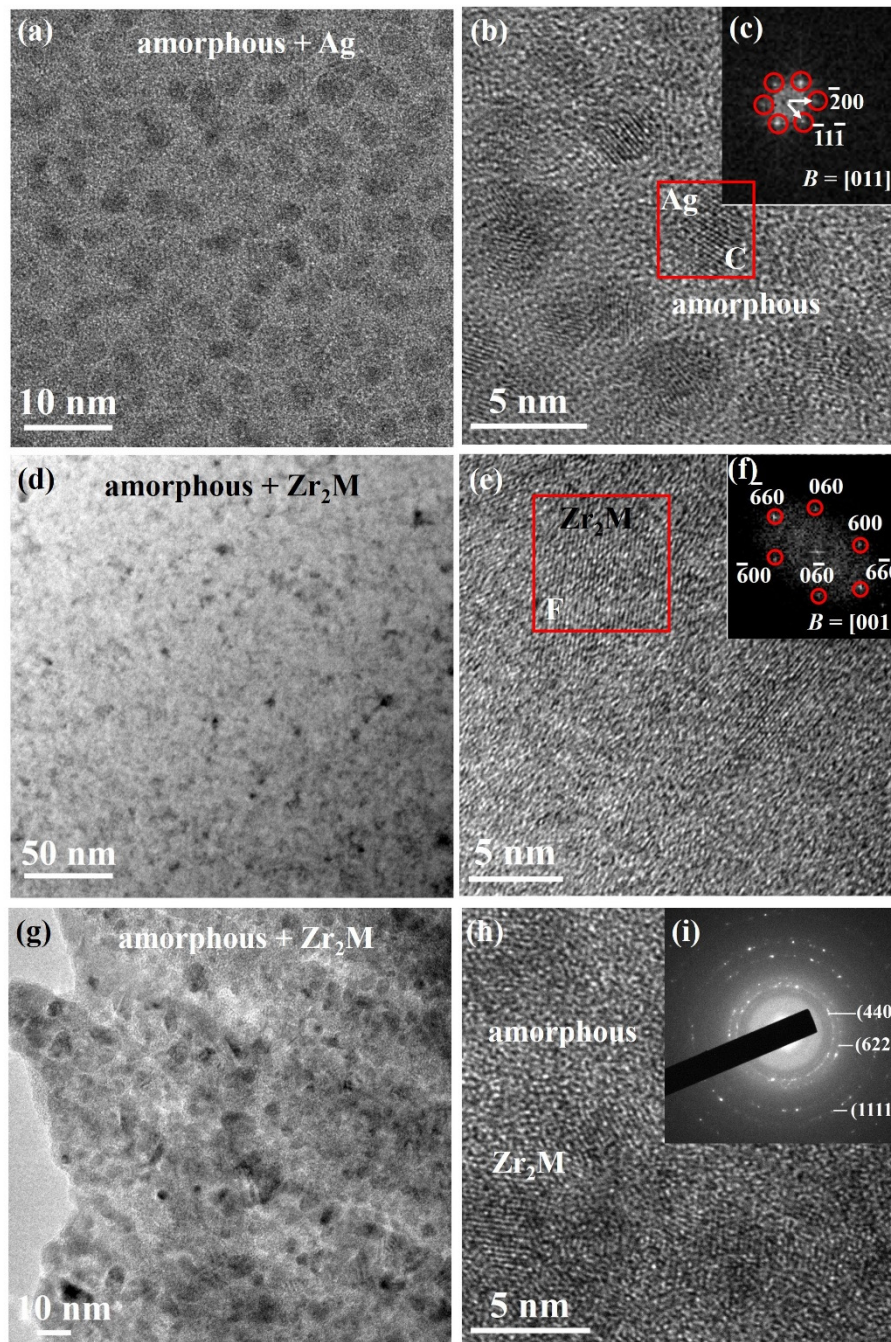


Fig. 4 Bright -field and high resolution TEM (HRTEM) images (a, b, d, e, g, h), selected-area electron diffraction patterns of (i) and fast Fourier-transform (FFT) patterns of: (c) Zone C and (f) Zone F for Group A, B, and C specimens prepared solely by ion milling. Group A: a-c, Group B: d-f, Group C: g-i

TEM specimens of Group D and E specimens are both dimpled to just perforate and then ion milling at a low ion beam energy. A typical HRTEM image and SAED pattern of the specimen in Group D are shown in Fig. 5(a-c), confirming the amorphous structure. TEM examinations of Group E specimen indicates that no “visible” microstructure changes occur in these specimens and the SAED pattern (Fig. 5f) shows a typical halo ring without detectable diffraction spots, confirming the amorphous structure of $Zr_{65}Al_7Co_7Ag_7Fe_7Ni_7$ alloy ribbon. Slight brightness contrast in the HRTEM

image (Fig. 5(d-e)) is probably due to non-uniform thickness of TEM specimen resulting from dimple and ion milling. XRD patterns shown in Fig. 1(a) indicate that the two as-spun alloy ribbons are both in a single amorphous phase. Thus, it can be determined that the TEM specimens of Groups D and E are free of artefacts and show real structure of as-spun $Zr_{65}Al_{7.5}Co_{22.5}Ag_5$ and $Zr_{65}Al_7Co_7Ag_7Fe_7Ni_7$ alloy ribbons.

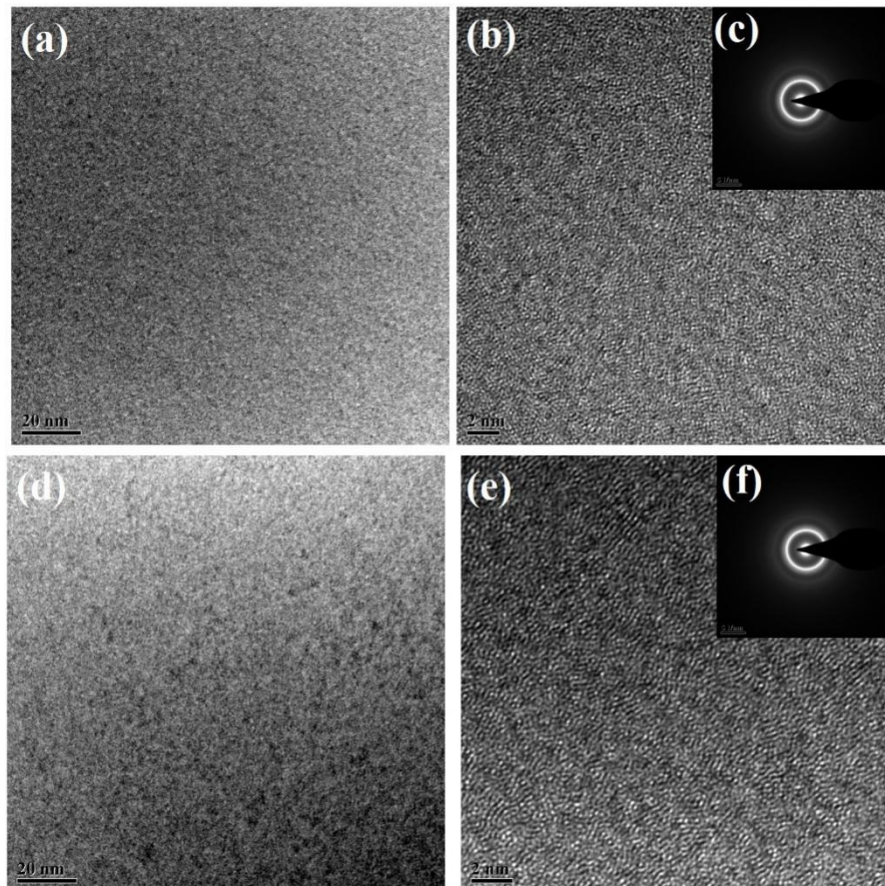


Fig. 5 Bright -field and high resolution TEM images and selected-area electron diffraction patterns of Group D and E specimens prepared by dimple and ion milling. Group D: a-c, Group E: d-f

4. Discussion

The specimen in Group A contains nanocrystallites phase coexistent with a small amount of amorphous phase, while the real structure is a single amorphous phase (Fig. 1, Fig. 5). Similarly, large crystalline particles can be found in Groups B and C, but the structure of $Zr_{65}Fe_7Co_7Ni_7Ag_7Al_7$ as-spun alloy ribbon is a solely amorphous phase (Fig. 1, Fig. 5). These contrast results suggest that the ion milling process accelerates the transformation from amorphous state to nanocrystal state. After examining various specimens in each group, it is found that distinct heating effect exists, even though the liquid nitrogen cold stage is always used and ion milling chamber temperature is 99K in the control up and down. Unfortunately, the present cold-stage is not enough to prevent the sample from local heating. Indeed, any instantaneous high temperature excursion is liable to heat the materials during ion milling and cooling to liquid nitrogen temperature does not provide an acceptable palliative^[18].

It is particularly noticed that the precipitates in amorphous phase formed during ion milling process for $Zr_{65}Al_{7.5}Co_{22.5}Ag_5$ amorphous alloy is entirely different from the phases formed after annealing. The difference in phases implies that the heating effect during ion milling could be more complicated than those in the sample after annealing.

$Zr_{65}Al_7Co_7Ag_7Fe_7Ni_7$ amorphous alloy ribbon is annealed at 750K for prolonging annealing time to 14.4ks, there are still no changes in XRD patterns as shown in Fig. 6. Similar phenomenon has been reported for related pseudo-high entropy glassy alloys. It is proved that $Zr_{65}Al_7Co_7Ag_7Fe_7Ni_7$ alloy is so stable to keep amorphous structure when even after the long time annealing below 750K. When annealing temperature reaches 970K (fig. 3), fcc- $Zr_2M+Zr_2Al_3+ZrAg+Al_{13}Co_4+Al_3Zr+Zr_6CoAl_2$ are formed instantly within a few minutes. Ion milling-induced fcc- Zr_2M is one of the phases formed upon annealing treatment indicating that during ion milling with the above described parameters for $Zr_{65}Al_7Co_7Ag_7Fe_7Ni_7$ amorphous alloy, the local heating temperature exceeds 750K and is lower than 970K.

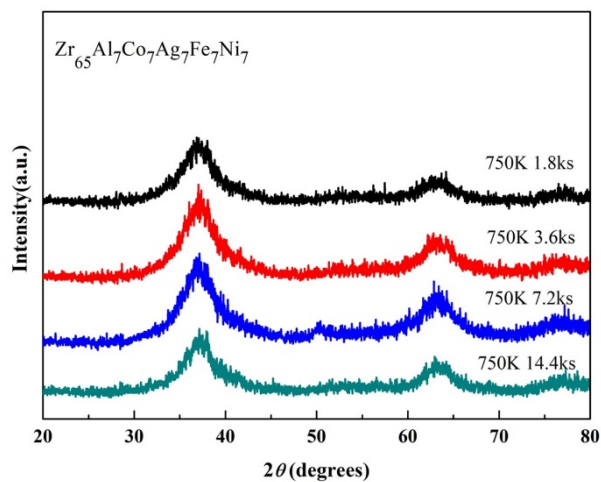


Fig. 6 X-ray diffraction patterns of $Zr_{65}Al_7Co_7Ag_7Fe_7Ni_7$ alloy ribbons annealed at a temperature above the first exothermic peak for 1.8ks, 3.6ks, 7.2ks and 14.4ks

The present results demonstrate the importance of careful control for TEM specimen preparation conditions. Compared data for Group A with that in Group D (Fig. 4(a-c), Fig. 5(a-c)), decreasing ion beam energy and gun angle during ion milling is better for preparing amorphous thin foils. Milling time of Group C is as long as 8.5h. Even though the ion beam energy is as low as 2Kev, we can easily recognize large crystalline particles (Fig. 4(g-I)). In order to reducing thinning time, samples of Groups D and E are dimpled before ion milling. Overall, pre-thinning methods and reducing milling time are also significant.

Basically, negative heats of mixing among components are required to obtain an alloy with high glass forming ability. If negative heats of mixing differ considerably in their values or a positive heat of mixing exists between the two components, phase separation becomes possible in the amorphous structure, leading to the formation of crystals. From Table2, it can be seen that Ag has large positive heats of mixing with Fe, Co, and Ni (28kJ/mol, 19kJ/mol, 15kJ/mol, respectively), suggesting the possibility of phase separation in the amorphous phase for $Zr_{65}Al_{7.5}Co_{22.5}Ag_5$ and $Zr_{65}Al_7Co_7Ag_7Fe_7Ni_7$ alloys. Phase separation is a metastable state. It has been discussed above that the local heating temperature exceeds 750K and the heated state provides the decomposition to form Ag-rich and Ag-poor areas. With the degree of Ag-enrichment, this Ag-rich structure is probably transformed into Ag crystallites.

Table 2 The values of $\Delta H_{(AB)}^{mix}$ (KJ/mol) cited from Akira Takeuchi and Akihisa Inoue's paper^[19]

(a) \ (b)	Zr	Fe	Co	Ni	Ag	Al
Zr	-	-16	-25	-30	-20	-44
Fe		-	-1	-2	28	-11
Co			-	0	19	-19
Ni				-	15	-22
Ag					-	-4
Al						-

5. Conclusions

(1) It was demonstrated that ion milling-induced structure changes from amorphous phase to amorphous+fcc-Ag for $Zr_{65}Al_{7.5}Co_{22.5}Ag_5$ and amorphous+fcc-Zr₂M for $Zr_{65}Al_7Co_7Ag_7Fe_7Ni_7$ amorphous alloys, even though the ion beam energy is as low as 2Kev. Completely different crystalline phases are formed after ion milling as compared with that after annealing.

(2) By comparing XRD patterns, HRTEM images, SAED patterns of the samples after ion milling with the samples after annealing, the locally heated peak temperature of TEM specimens is estimated to exceed 750K and be lower than 970K.

The operation parameters of ion milling should be carefully selected to avoid artefacts and wrong judgements. On the other hand, ion milling technique can be developed to synthesize a nanostructured layer on some BMGs' surface to obtain improved ductility, superior soft magnetic properties and other specific functions. Choosing a low ion beam energy and proper penning angle, we can get nanocrystalline surface layer with useful engineering properties just in a short period of time.

Acknowledgements

The authors are grateful for support from the National Natural Science Foundation of China (51771131).

References

- [1]. H YANG, X CHANG, W HOU, et al. TEM Specimen Preparation for Al-based Amorphous Alloys[J]. Materials Sciences Technology, 2006, 22(5): 655–658.
- [2]. X Gu, W Hao, J Wang, et al. Microstructure Changes in Zr-Based Metallic Glass Induced by Ion Milling[J]. Rare Metal Materials and Engineering, 2010, 39(10): 1693–1696.
- [3]. E, Snoeks, K, et al. Stress relaxation in tungsten films by ion irradiation[J]. Applied Physics Letters, 1997, 71(2): 267-269.
- [4]. Lotnyk A, Poppitz D, Ross U, et al. Focused high- and low-energy ion milling for TEM specimen preparation[J]. Microelectronics Reliability, 2015, 55(9-10): 2119-2125.
- [5]. Park Y M, Ko D S, Yi K W, et al. Measurement and estimation of temperature rise in TEM sample during ion milling[J]. Ultramicroscopy, 2007, 107(8): 663-668.
- [6]. Hsueh C H, Lee S. Effects of viscous flow on residual stresses in film/substrate systems[J]. Journal of Applied Physics, 2002, 91(5): 2760-2765.
- [7]. Wang Q, Cui Y Y, Ding N, et al. Metastable phase formation and transformation studied by ion mixing and computation for the Cu–Zr–Ni system[J]. Nuclear Instruments & Methods in Physics Research, 2013, 307: 111-114.
- [8]. Inoue A, Wang Z, Louzguine-Luzgin D V, et al. Effect of high-order multicomponent on formation and properties of Zr-based bulk glassy alloys[J]. Journal of Alloys and Compounds, 2015.
- [9]. Y. N, Guo, A, et al. Influence of Ag replacement on the formation and heating-induced phase decomposition of $Zr_{65}Al_{7.5}Co_{27.5-x}Ag_x$ ($x=5$ to 20at%) glassy alloys - ScienceDirect[J]. Journal of alloys and compounds, 783: 545-554.

- [10]. Marshall D B . Mechanisms of Failure from Surface Flaws in Mixed-Mode Loading[J]. Journal of the American Ceramic Society, 1984, 67(2).
- [11]. Qin X M , Tan J , Li C J , et al. On the formation, mechanical properties and crystallization behaviors of a $Zr_{56}Co_{24}Al_{20}$ bulk metallic glass[J]. Journal of Alloys & Compounds, 2015, 647:204-208.
- [12]. Louzguine D V , Inoue A . Multicomponent metastable phase formed by crystallization of Ti–Ni–Cu–Sn–Zr amorphous alloy[J]. Journal of Materials Research, 1999, 14(11):4426-4430.
- [13]. J. C , QIAO, and, et al. Isochronal and isothermal crystallization in $Zr_{55}Cu_{30}Ni_5Al_{10}$ bulk metallic glass[J]. Transactions of Nonferrous Metals Society of China, 2012, 22(3):577-584.
- [14]. Li M M , Inoue A , Han Y , et al. Influence of Ag replacement on supercooled liquid region and icosahedral phase precipitation of $Zr_{65}Al_{7.5}Ni_{10}Cu_{17.5-x}Ag_x$ ($x = 0-17.5$ at%) glassy alloys[J]. Journal of Alloys and Compounds, 2017,735:1712-1721.
- [15]. Ding J , Inoue A , Kong F L , et al. Phase decomposition and mechanical properties of pseudo-high entropy $Zr_{65}(Al,Fe,Co,Ni,M)_{35}$ ($M=Cu, Ag$ or Pd) glassy alloys[J]. Journal of Alloys and Compounds, 2020, 829:154513.
- [16]. Saida J , Matsushita M , Inoue A . Nano-Metals I. Nano Icosahedral Quasicrystalline Phase in $Zr_{65}Al_{7.5}Ni_{10}Ag_{17.5}$ Quaternary Glassy Alloy[J]. Materials Transactions, 2001, 42(8):1493-1496.
- [17]. Inoue A , Kong F L , Zhu S L , et al. Peculiarities and usefulness of multicomponent bulk metallic alloys[J]. Journal of Alloys & Compounds, 2016:707:12-19.
- [18]. Louzguine-Luzgin D V , Yavari A R , Vaughan G , et al. Clustered crystalline structures as glassy phase approximants.[J]. Intermetallics, 2009, 17(7):477-480.
- [19]. Takeuchi A , Inoue A . Classification of Bulk Metallic Glasses by Atomic Size Difference, Heat of Mixing and Period of Constituent Elements and Its Application to Characterization of the Main Alloying Element[J]. Materials Transactions, 2005, 46(12):2817-2829.